Advancing Bioluminescence Imaging Technology for the Evaluation of Anticancer Agents in the MDA-MB-435-HAL-Luc Mammary Fat Pad and Subrenal Capsule Tumor Models

Cathy Zhang, Zhengming Yan, Maria E. Arango, Cory L. Painter, and Kenna Anderes

Abstract

Purpose: Tumors grafted s.c. or under the mammary fat pad (MFP) rarely develop efficient metastasis. By applying bioluminescence imaging (BLI) technology, the MDA-MB-435-HAL-Luc subrenal capsule (SRC) model was compared with the MFP model for disease progression, metastatic potential, and response to therapy.

Experimental Design: The luciferase-expressing MDA-MB-435-HAL-Luc cell line was used in both MFP and SRC models. BLI technology allowed longitudinal assessment of disease progression and the therapeutic response to PD-0332991, Avastin, and docetaxel. Immunohistochemical analysis of Ki67 and CD31 staining in the primary tumors was compared in these models. Caliper measurement was used in the MFP model to validate the BLI quantification of primary tumors.

Results: The primary tumors in MDA-MB-435-HAL-Luc MFP and SRC models displayed comparable growth rates and vascularity. However, tumor-bearing mice in the SRC model developed lung metastases much earlier (4 weeks) than in the MFP model (>7 weeks), and the metastatic progression contributed significantly to the survival time. In the MFP model, BLI and caliper measurements were comparable for quantifying palpable tumors, but BLI offered an advantage for detecting the primary tumors that fell below a palpable threshold and for visualizing metastases. In the SRC model, BLI allowed longitudinal assessment of the antitumor and antimetastatic effects of PD-0332991, Avastin, and docetaxel, and the results correlated with the survival benefits of these agents.

Conclusions: The MDA-MB-435-HAL-Luc SRC model and the MFP model displayed differences in disease progression. BLI is an innovative approach for developing animal models and creates opportunities for improving preclinical evaluations of anticancer agents.

Cancer metastasis is the most lethal attribute of human malignancy and remains an ongoing therapeutic challenge for cancer drug discovery (1). The metastatic process depends on multiple factors, such as the composition of the tumor microenvironment, the characteristics of the primary tumor, and the compatibility of the distant organ that influences the metastatic growth (2). Future cancer therapies should be aimed at identifying specific targets that not only inhibit primary tumor growth but also reduce the spread of tumor cells into secondary sites, which leads to metastases (3). The development of therapeutic strategies for preventing the advancement of cancer metastasis requires a strong understanding of the underlying biological processes as well as the development of animal models that recapitulate the complexities of cancer metastatic progression.

Historically, animal models of metastasis were created using two methods described as experimental or spontaneous (4, 5). Experimental metastasis involves directly injecting tumor cells into the vasculature, and metastatic disease arises when cells "settle" into various anatomic locations. Spontaneous metastases arise from grafted primary tumors when tumor cells disseminate into the circulation and invade other organs and tissues, which is more reflective of actual disease progression. For the purpose of high-throughput drug screens, s.c. grafted tumor models are often used. However, s.c. grafted tumor models rarely develop spontaneous metastases (2, 4) and, additionally, they often fail to represent the anatomic location of origin for most neoplasms. Various orthotopic tumor models were developed by implanting human tumor cells (6) or tumor fragments (7) into the correct anatomic sites of immunocompromised mice. Compared with tumors in the subcutis, orthotopic models exhibited a higher metastatic potential and offered the advantages of more relevant host–tumor interactions, organ-specific growth environment, and drug exposure that closely reflects human cancer. However, due to the large variations in metastatic frequency (8) and kinetics, orthotopic

Authors' Affiliation: Department of Cancer Biology, Pfizer Global Research and Development, La Jolla Laboratories, San Diego, California

Received 4/7/08; revised 8/29/08; accepted 9/2/08.

The costs of publication of this article were defrayed in part by the payment of page charges. This article must therefore be hereby marked *advertisement* in accordance with 18 U.S.C. Section 1734 solely to indicate this fact.

Note: All authors are present or former employees of Pfizer.

Requests for reprints: Cathy Zhang, Department of Cancer Biology, Pfizer Global Research and Development, 10724 Science Center Road, San Diego, CA 92121. Phone: 858-622-3125; Fax: 858-622-5999; E-mail: cathy.zhang@pfizer.com.

doi:10.1158/1078-0432.CCR-08-0897

Translational Relevance

Cancer metastasis presents an ongoing challenge for modern drug discovery. Recent advances in optical imaging technology provide great opportunities for researchers developing animal disease models that recapitulate the complexities of human cancer and metastatic progression. Here, we applied bioluminescence imaging (BLI) technology to characterize the MDA-MB-435-HAL-Luc subrenal capsule and mammary fat pad mouse tumor models. Compared with the MDA-MB-435-HAL-Luc mammary fat pad model, the subrenal capsule model exhibited more efficient, spontaneous metastasis, which significantly affected the mouse survival time. We then tested three antineoplastic agents in both tumor models. Two of them, docetaxel and Avastin, have proven effective for treating metastatic cancer patients. BLI allowed quantitative assessment of the antitumor and antimetastatic efficacy of PD-0332991, Avastin, and docetaxel. BLI is a sensitive, noninvasive tool for longitudinal assessment of tumorigenesis, metastasis, and therapeutic intervention in animal models. By using optimized BLI technique, clinically relevant disease models can be developed for efficient evaluation of drug effects, thereby allowing scientists to gain deeper knowledge of the underlying biology during disease progression and to accelerate cancer drug discovery.

tumors often need to be surgically resected or selected by multiple passages *in vivo* (6, 9) to enhance the formation of distant metastases before mice succumb to the primary tumor burden (10, 11).

In this report, our work focused on developing disease models using the MDA-MB-435-HAL-Luc tumor cell line. MDA-MB-435 has been reported to possess a gene expression pattern characteristic of melanoma (12) but is often recognized as a metastatic human breast cancer line (13–15). The existing data (5, 16) indicate that MDA-MB-435 mouse models growing s.c. rarely display metastases, and mammary fat pad (MFP)-grafted tumors required surgical resection to develop efficient lung metastases (17). The MDA-MB-435-HAL line was derived from the MDA-MB-435 line for increased metastatic potential (18). The luciferase-expressing line, MDA-MB-435-HAL-Luc, was reported to exhibit metastasis in bones, lungs, and lymph nodes when inoculated intraventricularly or i.v. (19, 20). However, an experimental metastasis model omits the first steps of the metastatic cascade and does not represent the continuous release of tumor cells into the vasculature from the primary source. Here, the MDA-MB-435-HAL-Luc subrenal capsule (SRC) tumor model was explored due to a higher potential for the development of spontaneous metastasis (21).

The SRC model was developed for assessing tumor growth from a clinical patient and the response to therapy in a mouse model (22). Because the kidney is a highly perfused organ, tumors growing under the SRC have the advantage of accessing nutrients, drugs, and other substances in circulation. Previous studies have shown that grafts in the SRC exhibited reproducible growth rates and retained the morphologic and malignant characteristics of the parent tumors (23). The SRC model was applied to predict the clinical response to chemotherapy (24, 25). Although SRC tumor models have been widely used in the past, the assessment of end points was often limited to the analysis of selected tissues at the completion of an experiment rather than during the longitudinal progression of the disease course. We applied noninvasive bioluminescence imaging (BLI) technology to circumvent this issue.

Optical imaging, either bioluminescent or fluorescent, has emerged as a sensitive, cost-effective, and quantitative imaging modality that provides the capacity to conduct noninvasive longitudinal studies monitoring tumorigenesis, metastasis, and responsiveness to anticancer agents in living mice (26, 27). The common approach for *in vivo* optical imaging is to genetically encode luciferase or fluorescent proteins (usually green fluorescent protein) into an animal organ or tumor cells so that the molecular or cellular events can be visualized and tracked noninvasively during cancer disease progression. BLI output is generated by the enzymatic reaction of luciferase with the substrate luciferin whereas fluorescent light emission requires excitation by an external light source. The advantage of *in vivo* fluorescence imaging (FLI) over BLI is the flexibility to produce light from either intrinsically produced probes or exogenously injected probe(s) whereas whole-body BLI solely relies on the reaction of the endogenous luciferase with the injected substrate (luciferin; ref. 28). By using two or more spectrally distinct fluorescent probes, FLI allows multicolor imaging to track multiple molecular or cellular events simultaneously (29, 30). On the other hand, FLI generally allows visualization of both metabolically active and inactive cells whereas BLI has the benefit of only monitoring viable cells. Thus, *in vivo* BLI was found to be a more reliable indicator of cell fate in real time (26, 31, 32) as in the case of monitoring micrometastasis and immune cell trafficking. Each of the BLI and FLI modalities has unique applications and limitations, and the sensitivities of either system were found to be associated with the instrumental and probe designs (33). Researchers have to weigh the trade-offs based on the specific purpose of the study to make a choice between the FLI-based and BLI-based systems.

This report describes the application of BLI technology to characterize the SRC and MFP mouse tumor models using a luciferase-expressing MDA-MB-435-HAL-Luc cell line. Because multiple factors affect the bioluminescence signal intensity, diligent optimization and validation was done to reliably deploy this tool for longitudinal evaluation of disease progression and response to anticancer agents. BLI revealed differences in the disease progression in these two models and provided quantitative assessment of antitumor activity for PD-0332991 (cyclin-dependent kinase inhibitor), Avastin, and docetaxel against the primary and metastatic tumor burden.

Materials and Methods

The stable luciferase-expressing MDA-MB-435-HAL-Luc line, derived from the MDA-MB-435 cell line, was transfected as previously reported (19). The antibodies used in the immunohistochemical assays included anti-CD31-PECAM-1 (Santa Cruz Biotechnology; sc-1506, dilution 1:20) and anti-Ki67 (Lab Vision; RM-9106, dilution 1:800).

In vivo *studies*. All animal husbandry and experimental procedures conducted in this study complied with the Guide for the Care and Use

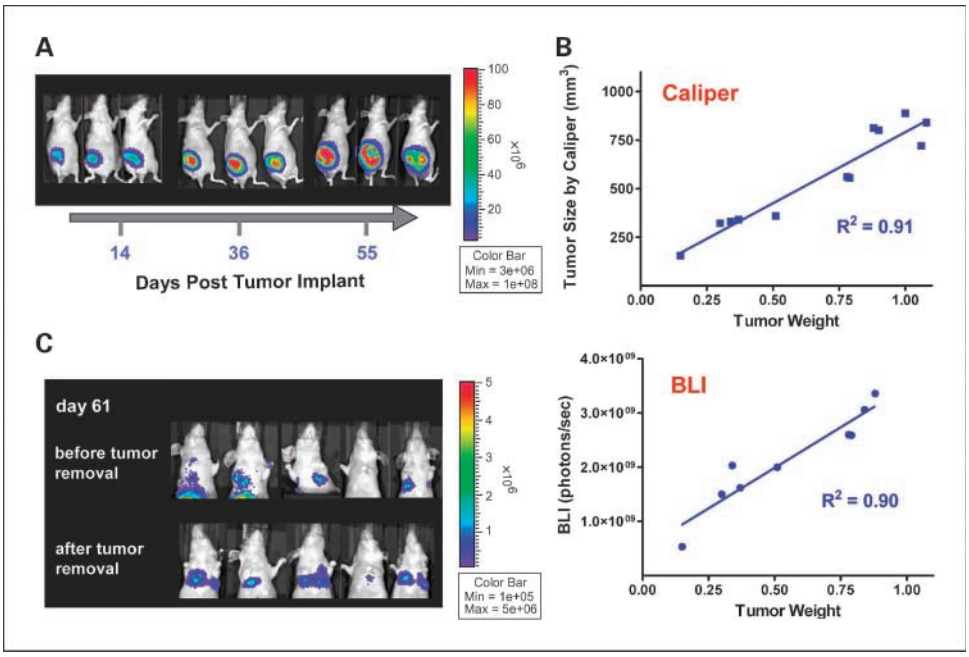

Fig. 1. Tumor growth and distant dissemination to the lungs in the MDA-MB-435-HAL-Luc MFP model. The imaging was captured at the peak time after i.p. injection of 150 mg/kg D-luciferin. *A,* on selected days, BLI of 3 representative mice (10 total) showing primary tumor growth under the MFP during the disease course. The imaging exposure time was 5 s. *B,* at necropsy, the weights of tumors from the MDA-MB-435-HAL-Luc MFP model exhibited a strong linear relationship between caliper assessment ($R^2 = 0.91$) and BLI quantification ($R^2 = 0.90$). *C,* BLI revealed tumor cell dissemination in the lungs on day 61, both before and after removal of the primary tumor. The imaging exposure time was 60 s.

of Laboratory Animals (Institute for Laboratory Animal Research, 1996) and were approved by the Pfizer Global Research and Development Institutional Animal Care and Use Committee. Mice were obtained from Charles River Breeding Laboratories and acclimatized for a 72-hr period before use.

MFP-implanted tumor model. Female athymic NCr-*nu*/*nu* or SCID beige mice were used for this model. The mice were anesthetized with 2.5% isofluorane before implanting tumors. Tumor cells (2×10^6) growing in the midlogarithmic phase were suspended in 100 μL PBS with 50% (volume for volume) Matrigel (VWR; cat no. 47743-714) and implanted under the MFP of mice. Tumor sizes in this model can be assessed either by BLI or caliper measurements. Before dosing with cancer agents, the mice were randomized into different groups with the same mean tumor volume. The tumors were measured twice weekly with calipers or once weekly with BLI. The tumor volume was calculated as $0.5 \times (\text{length} \times \text{width}^2)$.

SRC tumor model. SCID beige or NIH3 nude mice were anesthetized with an i.p. injection of ketamine (100 mg/kg)/xylazine (6 mg/kg) before surgery. The left kidney of the mouse was accessed through a small flank incision and was lifted above the incision site (22). A trocar fragment of MDA-MB-435-HAL-Luc (1-2 mm^3) was loaded into a 16-gauge needle and inserted beneath the renal capsule. The kidney was returned back into the body cavity. The incisions in the muscle and skin layers were closed sequentially with 6-0 surgical nylon sutures. Treatment started at 14 d after the tumor implant when the mice were randomized into different groups with the same mean BLI.

Anticancer agents and* in vivo *administration. PD-0332991 was synthesized by Pfizer chemists and prepared as previously described

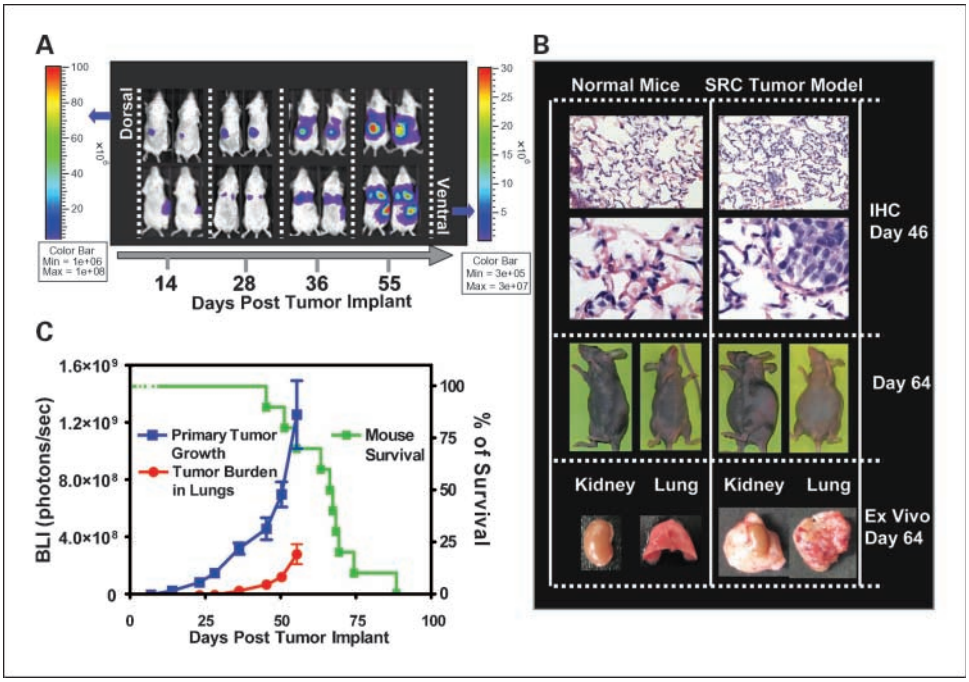

Fig. 2. Tumor growth and distant dissemination to the lungs in the MDA-MB-435-HAL-Luc SRC model. *A,* on selected days, BLI of 2 representative mice (15 total) revealed cancer progression during the course of the disease. Dorsal (*top*) and ventral (*bottom*) views of mice were imaged separately for 2 and 60 s, respectively. The imaging color bar was set up separately for primary tumors and metastasis due to the difference in intensities. *B,* various assessments showing disease progression in the SRC tumor – bearing mice. A normal mouse is used for reference. On day 46, a histologic analysis (H&E staining) showed tumor cell infiltration in the lungs (*top*). Macroscopic examination showed that mice at late stages of the disease experienced severe edema due to disease progression (*middle*). At euthanasia, the tumor burden on the kidney and lungs were collected from moribund mice (*bottom*). *C,* quantitative assessment of the primary tumor (*blue*), tumor cell dissemination in the lungs (*red*) via BLI (mean ± SE). A Kaplan-Meier survival plot (*green*) of mice (median) showed disease progression in the MDA-MB-435-HAL-Luc SRC model. Data in this graph was collected from a group of 15 mice.

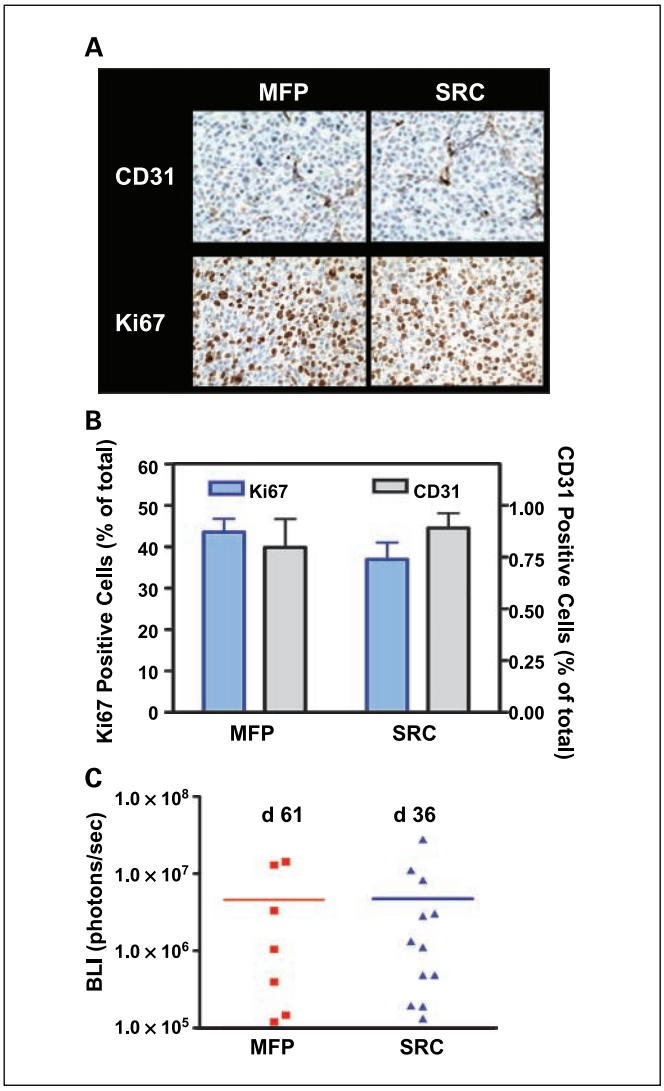

Fig. 3. Comparison of tumor growth at primary and secondary (lung) sites between the MDA-MB-435-HAL-Luc MFP and SRC models. Immunohistochemical examination (*A*) and quantification (*B*) showed that comparable tumor proliferation indices (Ki67) and vascular densities (CD31) were observed in these two models. *C,* BLI of the lung tumor burden in the SRC model on day 36 are comparable with those in the MFP model on day 61.

(34). Avastin and docetaxel (Taxotere) were purchased from Henry Schein (cat. no. 2237867 and 1027647) and prepared following the manufacturer's instructions. When tumors reached the desired size, the mice were treated as follows: group 1, vehicle; group 2, PD-0332991 at 200 mg/kg via oral gavage twice each week for 3 wk; group 3, Avastin at 15 mg/kg via i.p. once each week for 7 wk; and group 4 and 5, docetaxel at 15 and 30 mg/kg via i.p. once each week for 2 wk. The same dose(s) and dosing regimen for each agent were used in both the MDA-MB-435-HAL-Luc MFP and SRC models. No adverse effects were observed in mice treated with PD-0332991, Avastin, and docetaxel using the indicated dosing regimen.

Bioluminescence imaging. *In vivo* BLI was conducted on the IVIS100 system with the use of the Living Image acquisition and analysis software (Caliper Life Sciences). Before imaging, the mice were anesthetized with 2.5% isofluorane and i.p. administered with 150 mg/kg D-luciferin firefly potassium salt (Caliper Life Sciences). Serial imaging of the tumor burden was done between 10 and 20 min after injection of luciferin to capture the peak intensities, which seemed to best represent tumor volume. Signal intensity was quantified as the sum of all detected photon counts within an oval shaped region of interest that was selected manually over the tumor or metastasis region, and the area quantified was kept constant at each time point. In the MFP model, the mice were imaged ventrally for 5 and 60 s to detect the primary tumor and metastasis in lungs, respectively. To image lung metastasis before the removal of the primary tumor, the lower portion of the mouse was shielded before imaging to minimize the signal interference from the primary tumor. In the SRC model, the mice were imaged dorsally for 5 s and ventrally for 60 s to detect the primary tumor and lung metastasis, respectively.

Histopathology. Tumors or lungs were excised from the mice at necropsy and were preserved in a 10% formalin solution (Sigma) before transferring to 70% ethanol at 24 hr. Tissues were prepared as previously described (35) for histopathology (paraffin preparation, sectioning, and H&E staining) and analyzed using the Chromovision automated cell imaging system.

Data analysis. The data in this report are shown as mean values ± SE. Statistical analyses were conducted with the Prism GraphPad software (GraphPad) for one-way ANOVA followed by the Dunnet's *t* test. The BLI results or the tumor sizes were compared between the vehicle and drug-treated groups on specific dates to assess significant differences.

Results

Tumor progression and dissemination in the lungs using a MDA-MB-435-HAL-Luc MFP model. Tumors growing in the MDA-MB-435-HAL-Luc MFP model can be measured via caliper measurements or BLI. Figure 1A displays the imaging of 3 representative mice at different time points throughout the disease course. For validation of the study, the tumor weights in different ranges were obtained at necropsy after data acquisition via caliper and BLI. A strong linear relationship ($R^2 = 0.91$) was observed between caliper assessment and resected tumor weight up to 1.1 g whereas the linear relationship ($R^2 = 0.90$) between BLI and tumor weight was only maintained below 0.87 g (Fig. 1B). BLI measurements for large tumors (>0.87 g) were excluded from the plot as they were out of the linear range. As the primary tumor reaches 800 to 1,000 mm^3, spontaneous metastasis in the lung was seen in >90% of the mice when the primary tumor was shielded with a black metal block. In some cases, the primary tumors grew too large and came close to the body surface, causing signal scatter from the primary tumor to interfere with the signal from the metastatic lesions. To aid visualization of tumor dissemination in the lungs, the mice were imaged after the primary tumors were surgically resected. Figure 1C displays the visualization of lung metastases in 5 representative mice before and after the surgical removal of the primary tumors.

Tumor progression and dissemination in the lungs using a MDA-MB-435-HAL-Luc SRC model. Once the MDA-MB-435-HAL-Luc tumor trocar fragments were implanted under the SRC, tumors were visualized via BLI. The dorsal and ventral view of each mouse was imaged once weekly throughout the disease course to monitor the progression of primary tumor and lung metastases, respectively. Spontaneous lung metastases were detectable at the 4th week post tumor implant. By day 28, tumor lesions in the lungs can be visualized in all mice (100%). The dorsal and ventral images of 2 representative mice at different time points (Fig. 2A) showed progression of the primary tumor and lung metastasis over time. H&E staining of the lungs collected on day 46 after tumor implantation confirmed tumor cell infiltration in the lungs (Fig. 2B, *top*).

Approximately 8 weeks after implanting the SRC tumors, tumor-bearing mice exhibited physiologic signs that were consistent with advanced metastatic disease, such as labored breathing, severe edema, reduced appetite, and reduced mobility (Fig. 2B, *middle*). The moribund mice were euthanized for survival analysis. Figure 2B (*bottom*) shows a macroscopic view of the primary tumor (kidney) and the secondary tumor (lung) compared with the normal organs collected after euthanasia. The primary tumor sizes of the moribund mice at the survival end points were in the range of 1,000 to 1,500 mg, which was comparable with the tumor sizes of the MFP model at a similar time post-implant. The kinetics of primary tumor growth, the changes in the lung tumor burden, and mouse survival are shown in Fig. 2C. Tumor burdens at the SRC and the lungs, as measured by BLI, well predicted the individual mice survival time (data not shown).

Comparison of the MDA-MB-435-HAL-Luc MFP and SRC tumor models. At days 42 to 46 after tumor implantation, primary tumors were collected from the MDA-MB-435-HAL-Luc MFP tumor–bearing and SRC tumor–bearing mice for immunohistochemical analysis. The results showed that the intensities of Ki67 and CD31 staining were comparable between the MFP and SRC tumors (Fig. 3A, *B*), indicating similarities in tumor growth rate and vascularity. BLI quantification indicated that the tumor burdens in lungs from MFP mice at day 61 were comparable with those from the SRC model at day 36 (Fig. 3C), suggesting there were differences in the kinetics of metastasis in these two models.

The therapeutic response of PD-0332991, Avastin, and docetaxel in the MDA-MB-435-HAL-Luc MFP model. Fourteen days after injection of MDA-MB-435-HAL-Luc tumor cells, mice with palpable tumors were randomized into four groups of seven each, with a mean tumor volume of ~160 mm^3 in each group. The mice were treated as described in Materials and Methods. Tumor sizes were assessed via caliper measurements or BLI. Significant efficacies were seen in all treated groups throughout the disease course by caliper measurement (Fig. 4A). Bioluminescence images on day 45 from 2 representative mice of each group confirmed the antitumor efficacies in all treated groups (Fig. 4B, *top*). Overall, a similar outcome (day 45) was observed between BLI and caliper measurements (Fig. 4C) except in the group treated with docetaxel at 30 mg/kg. On day 45, some mice treated with docetaxel (30 mg/kg) seemed tumor-free by visual assessment, but BLI quantification indicated that ~1.2% (compared with pretreatment) of tumor cells remained alive. On day 61, tumors in the vehicle-treated group reached the size limit (1,000-1,500 mm^3). The mice were imaged after surgical removal of the primary tumors. The images of 2 representative mice show the overall outcome (Fig. 4B, *bottom*). A scatter plot showed that tumor lesions in the lungs were detectable in all vehicle-treated mice (Fig. 4D). However, 4 of 7, 2 of 7, and 3 of 7 mice showed no signs of tumor dissemination in their lungs with PD-0332991 (200 mg/kg), Avastin (15 mg/kg), and docetaxel (15 mg/kg) treatment, respectively. Docetaxel at 30 mg/kg showed no detectable lung metastasis in any of the mice on day 61.

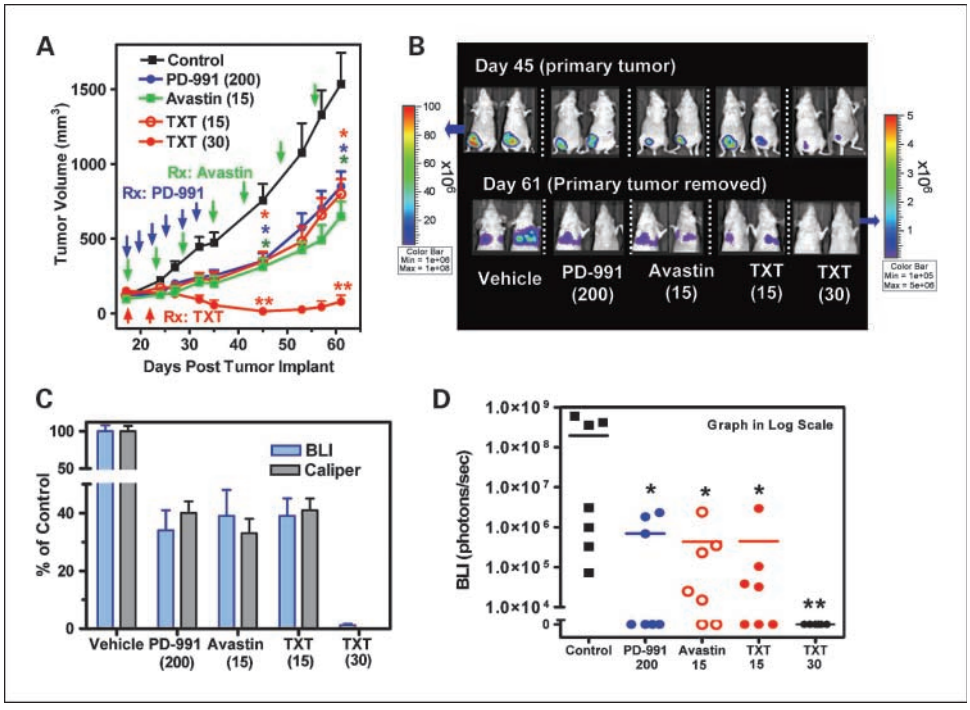

Fig. 4. Quantitative assessment of the therapeutic responses of PD-0332991, Avastin, and docetaxel (TXT) in the MDA-MB-435-HAL-Luc MFP model. Data in parentheses, the dose for each agent in treated groups (mg/kg). The dosing regimen is described in Materials and Methods. * and ** indicate that the treated group was significantly different from the control group ($P < 0.05$ and $P < 0.01$, respectively). *A,* caliper measurements showed the antitumor effects of PD-0332991 (200 mg/kg), Avastin (15 mg/kg, i.p.), and docetaxel (15 and 30 mg/kg, i.p.). *B,* BLI of the primary and secondary tumor (lung) from 2 representative mice on days 45 and 61 post – tumor implant, showing the therapeutic response of PD-0332991, Avastin, and docetaxel. Images of lung metastases were obtained on day 61 after the primary tumors were removed. The exposure time for imaging the primary tumor (day 45) and the lung metastases (day 61) was 5 and 60 s, respectively. *C,* comparison of the assessment of tumor size between the caliper measurements and BLI for all agents at tested doses. Values in graph, mean ± SEM. Data were normalized by designating the mean value in the control group as 100%. *D,* BLI quantitation of lung tumor burdens in mice treated with vehicle, PD-0332991, Avastin, or docetaxel.

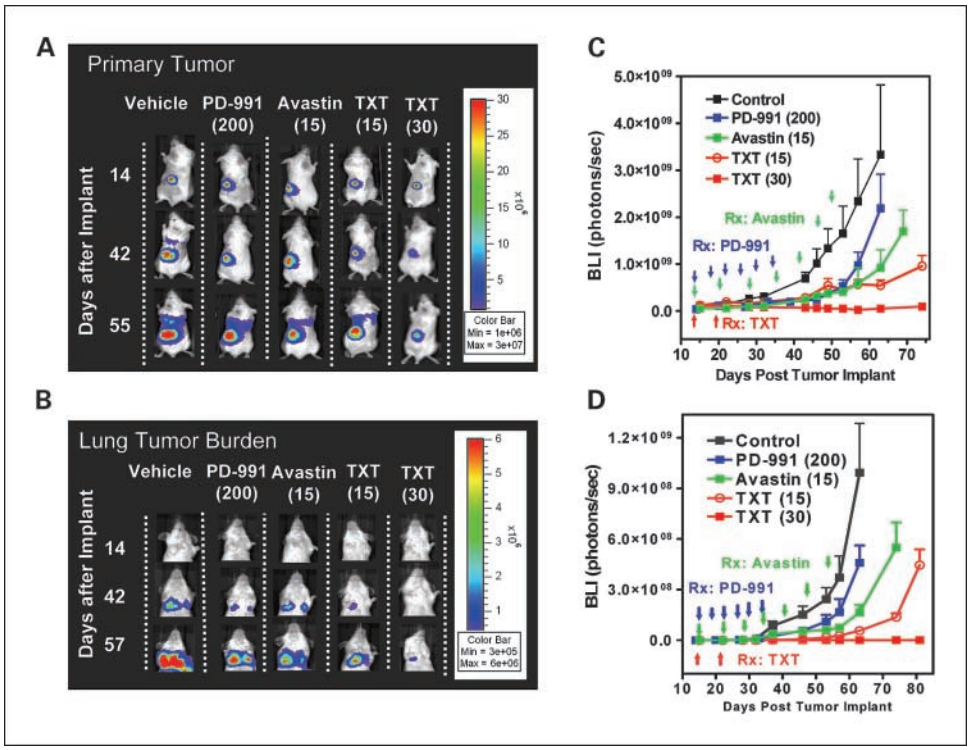

Fig. 5. Visualizing and quantifying the efficacies of PD-0332991, Avastin, and docetaxel (TXT) against the primary and secondary tumor in the MDA-MB-435-HAL-Luc SRC model. Data in parentheses, the dose for each agent in treated groups (mg/kg). The dosing regimen is described in Materials and Methods. BLI of the primary tumor growth (*A*) and of the secondary tumor growth in lungs (*B*) on selected days are shown throughout the disease course. One representative mouse was selected from each group (10 each) to show the overall outcome. Dorsal (*A*) and ventral (*B*) views of mice were imaged separately for 5 and 60 s, respectively. Measurements of the BLI show the benefits of treatment with PD-0332991, Avastin, and docetaxel against growth of the primary tumor (*C*) and of the secondary tumors in the lungs (*D*). Values in graph, mean ± SE.

The therapeutic response of PD-0332991, Avastin, and docetaxel in the MDA-MB-435-HAL-Luc SRC model. Fourteen days after MDA-MB-435-HAL-Luc tumor fragments were surgically implanted under the SRC, the mice were randomized into five groups of 13 each, based on the BLI of the primary tumor with a mean value at 6-7 $\times$ 10^6 photons/s in each group. After randomization, the mice were treated as described in the Materials and Methods section. The images of primary and secondary tumors from 1 representative mouse of each group on selected days are shown in Fig. 5A and B, respectively. As shown in Fig. 5C and D, the BLI output of the primary tumor growth and tumor dissemination in the lungs showed the antitumor and antimetastatic efficacies of these agents. On day 46, 3 mice from each group were euthanized, and lung tissues were collected for immunohistochemical analysis. H&E staining (Fig. 6A) showed the response of lung-infiltrating tumor cells to all agents, confirming the results of BLI analysis. At late stage of the disease course, moribund mice were sacrificed for survival analysis. The Kaplan-Meier plot displayed the overall survival benefits of each treatment (Fig. 6B). Table 1 summarizes the response of disease progression to therapy in the MDA-MB-435-Luc SRC tumor–bearing mice. BLI quantification of the primary tumors and the tumor burden in lungs predicted the survival benefit of PD-0332991, Avastin, and docetaxel (15 and 30 mg/kg) treatments in the MDA-MB-435-HAL-Luc SRC model.

Discussion

BLI has emerged as a powerful tool for the development of preclinical models (36, 37). In this report, we showed the advantage of BLI over the traditional approaches in allowing the quantitative and longitudinal assessment of dynamic disease progression and therapeutic intervention with cancer agents in luciferase-expressing MDA-MB-435-HAL-Luc MFP and SRC models. Because the IVIS100 produces depth-dependent planar images, the primary tumor and lung metastases in the SRC model were separately tracked by imaging mice in the dorsal and ventral positions. The newly developed tomographic optical systems are designed to overcome this disadvantage, but there is a trade-off between obtaining three-dimensional images of the malignancy and the system throughput. Planar BLI is an ideal tool for early drug-screening purposes due to its low cost and high-throughput features (27), and it has proven reliable for quantitative assessment of tumor burdens and metastases (38, 39).

For tumors that are measurable by calipers in the MDA-MB-435-HAL-Luc MFP model, the accuracies of BLI and caliper measurements were comparable (Fig. 1B). As the tumor burden grew beyond the limit (>0.87 g), BLI displayed higher variability and often did not reflect the real tumor size, consistent with a previously published report (38). When compared with the caliper-determined tumor volume, BLI output is thought to offer more accuracy because it is primarily derived from metabolically active tumor cells. However, BLI output in tumors relies on factors such as the ATP, O_2, and substrate (D-Luciferin) concentrations for the firefly reaction. Therefore, higher occurrences of necrosis, hypoxia, and heterogeneity in large tumors would affect the BLI output (37). Tumor location may also impact upon BLI intensity because the luciferin distribution varies in different organs or locations (40). For example, our data suggested that the quantification of large tumors (>0.87 g) in the MDA-MB-435-HAL-Luc SRC model was less variable with BLI, possibly because the tumor can easily access the substrate (D-Luciferin), compared with the location under the MFP. We conclude that application of BLI may not be necessary for measuring primary

tumors in the palpable range from the MFP tumor model, especially during the drug-screening process when the experimental procedures and data acquisitions are more time-consuming compared with caliper assessment. However, the benefit of BLI in the MDA-MB-435-HAL-Luc MFP model was the ability to track metastasis in live mice (Fig. 1C).

In the MDA-MB-435-HAL-Luc SRC tumor model, primary tumors and metastases are not accessible by calipers. BLI allowed monitoring of the disease progression and clearly had advantages over conventional approaches. The distinct advantage of the SRC model over the MFP model is that primary tumor growth and metastatic progression in the SRC model can be concurrently measured over the disease course. The primary tumor and metastatic tumor(s) in the SRC model were spatially distant from one another and could be viewed separately in both dorsal and ventral positions. Therefore, the interference between two signal sources was minimal compared with the MFP model. More importantly, the BLI of the secondary tumor burden in the lungs from the SRC model was 5-fold to 6-fold lower than the primary tumor during the disease course. By comparison, the MFP model exhibited a 3-log difference. Mice bearing MDA-MB-435-HAL-Luc SRC tumors showed tumor dissemination in the lungs at the 4th week, which was 3 weeks earlier than in the MFP model. Compared with tumors under the MFP, tumors in the SRC can easily gain access to the circulation and/or lymphatic systems, allowing the disseminated tumor cells to anchor in secondary sites at an early stage. In contrast, spontaneous lung metastasis in the MFP model required a longer time (7-9 weeks) to develop, and the progression significantly lagged behind the primary tumor. As shown in Fig. 3C, the BLI output from lung metastases of SRC tumor–bearing mice on day 36 had comparable intensities with that of MFP tumor–bearing mice on day 61, showing the difference between these two models in the kinetics of tumor cell dissemination into the lungs. However, based on the results of Ki67 and CD31 staining (Fig. 3A, *B*), the primary tumor under the MFP or SRC displayed similar growth rates and vascular properties. As the SRC tumor–bearing mice were sacrificed due to moribund conditions at a late stage of the disease course, gross examination indicated that the lungs were covered with infiltrated tumor tissues (Fig. 2B, *bottom*), suggesting that the deterioration of the health conditions could be mainly attributed to excessive tumor burden in the lungs. In comparison, mouse survival in the MFP model was limited only by the allowable primary tumor size (~1,500 mm^3), with minimal impact from the metastasis. The MDA-MB-435-HAL-Luc MFP and SRC models exhibited different metastatic potentials that affected the disease progression and the survival end points.

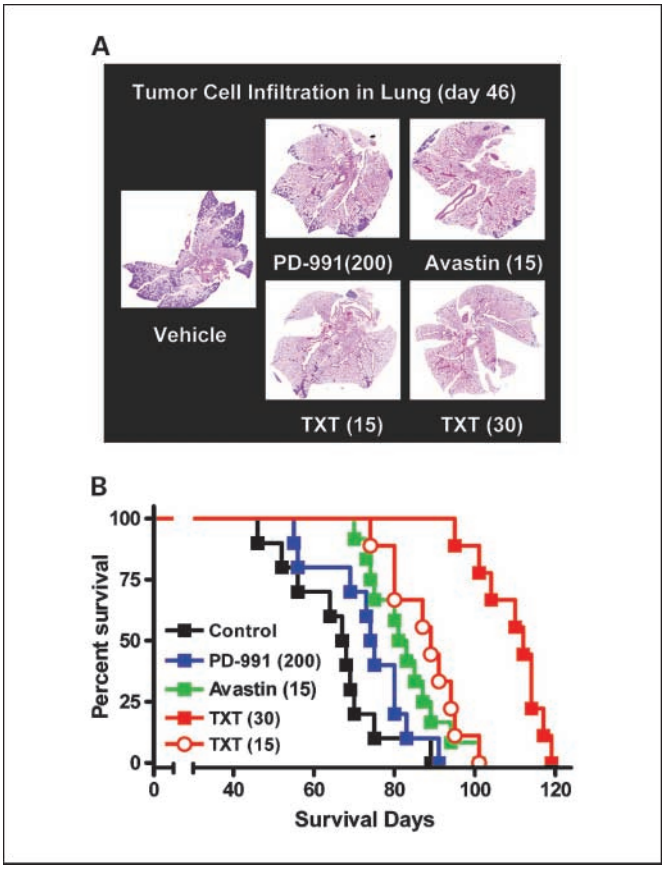

Fig. 6. Therapeutic response of the MDA-MB-435-HAL-Luc SRC model to PD-0332991, Avastin, and docetaxel. Data in parentheses, the dose for each agent in treated groups (mg/kg). The dosing regimen is described in Materials and Methods. *A,* on day 46 post – tumor implantation, H&E staining showed the tumor cells infiltrating into the lungs and the response to therapy. *B,* Kaplan-Meier survival curve shows that PD-0332991, Avastin, and docetaxel improved the mouse survival time in the MDA-MB-435-HAL-Luc SRC model.

The therapeutic response of PD-0332991, Avastin, and docetaxel was assessed in the MDA-MB-435-HAL-Luc MFP model. As primary tumors in the control group reached ~750 mm^3 (Fig. 4C), caliper measurements and BLI quantification displayed comparable benefits for each agent/dose, thus confirming that the accuracy of caliper measurements and BLI quantifications were similar. However, BLI offered a great advantage when tumors fell below a palpable size. When MDA-MB-435-HAL-Luc MFP tumor–bearing mice were treated with 30 mg/kg docetaxel, tumors were nearly invisible on day 45, but BLI revealed that 1.2% (compared with the initial quantity) of the tumor cells were still alive (Fig. 4C). The sensitive measurement of tumor cells/mass via BLI predicted that the tumor would eventually relapse. The direct measurements of relative tumor cell survival by BLI can potentially serve as surrogate pharmacodynamic end points to accurately measure the effects of drug treatments. In addition, BLI revealed the antimetastatic features of PD-0332991, Avastin, and docetaxel (Fig. 4D).

In the MDA-MB-435-HAL-Luc SRC model, immunohistochemical evaluation of the lungs collected on day 46 displayed tumor dissemination and were responsive to drug treatments. The immunohistochemical assessment was limited to qualitative information at a terminal time point and may not provide accurate quantitation. BLI enabled quantitative assessment of disease progression and the response to drug treatment throughout the disease course. Mice treated with PD-0332991 at 200 mg/kg showed significant changes in primary and secondary tumor growth on day 46 but not on day 63 (Table 1). Avastin (15 mg/kg) and docetaxel (15 and 30 mg/kg) treatments led to significant changes in the growth of primary tumors and secondary tumors in the lungs during the period from day 46 to 63. The Kaplan-Meier survival plot showed that Avastin and docetaxel significantly ($P < 0.05$) improved the mouse median survival time compared with the vehicle-treated mice (Table 1) whereas PD-0332991 only displayed a marginal

Table 1. *In vivo* efficacies of PD-0332991, Avastin, and docetaxel in MDA-MB-435-HAL-Luc SRC model

Agent* (dose in mg/kg)	% TGI against primary tumor †		% Inhibition of lung tumor burden		Median survival (d)
	day 46	day 63	day 46	day 63	
Vehicle	0	0	0	0	67.5
PD-991 (200)	71.2 ‡	36.4%	70.4% ‡	51.3%	74.5
Avastin (15)	68.5§	75.6 ‡	71.4% ‡	81.1%§	81 ‡
TXT (15)	66.5%§	83.5%§	97.1 %§	94.2%§	89§
TXT (30)	105%§	98.6%§	100%§	99.4%§	112§

Abbreviations: TGI, tumor growth inhibition; PD-991, PD-0332991; TXT, docetaxel.
*PD-0332991 was administered via oral gavages twice each week for 3 wk. Avastin was i.p. administered once each week for 7 wk. Docetaxel was administered via i.p. injection once each week for 2 wk.
† %TGI was calculated as 100 x (1-ΔT/ΔC). Changes in tumor volumes (Δ) for each treated (T) and control (C) group were calculated by subtracting the mean tumor volume on the 1st day of treatment from the mean tumor volume at the day of assessment.
‡ $P < 0.05$ (versus vehicle-treated group by one-way ANOVA followed by Dunnet's t test).
§ $P < 0.01$ (versus vehicle-treated group by one-way ANOVA followed by Dunnet's t test).

survival benefit ($P > 0.05$). BLI quantitation of the disease progression in treated and nontreated mice well predicted the mouse survival time. As a vascular endothelial growth factor–specific antibody, Avastin has been previously shown to significantly inhibit tumor microvessel formation in an MDA-MB-435 model via a dynamic contrast–enhanced magnetic resonance imaging test (41) and is expected to affect metastasis. This latter point agrees with the results of our study, indicating that long-term dosing of Avastin can significantly inhibit growth of the primary tumor and metastases. The Avastin treatment will ultimately increase mouse survival time in the MDA-MB-435-HAL-Luc SRC model. Docetaxel at 15 and 30 mg/kg also decreased the primary and secondary tumor burdens long after the treatment ended, resulting in a robust survival benefit. Based on published data, docetaxel induces cell death via apoptosis or mitotic catastrophe (42) and has been shown to induce tumor regression in many preclinical tumor models (43). As a cyclin-dependent kinase 4 or cell cycle inhibitor, PD-0332991 primarily induces tumor stasis in most model systems without causing cell death during the dosing period, and tumors often relapse after the treatment period ends (34). Therefore, mice bearing a SRC tumor treated with PD-0332991 failed to show benefits in the late stages of the disease (day 63). However, PD-0332991 at the same dose had significant benefits (Fig. 4) against the primary and secondary tumors from early-stage to late-stage (day 61) disease in MFP tumor–bearing mice. It is possible that not only the pharmacologic and pharmacokinetic properties of individual agents but also other variables, such as the biodistribution of the agent, the microenvironment of the tumor or lesion, the kinetics of the disease progression, and so on, can affect the therapeutic benefit of the agents in the MDA-MB-435-HAL-Luc MFP and SRC models. Despite the huge clinical success in treating metastatic cancer patients, docetaxel and Avastin were rarely tested in spontaneous metastasis models in the preclinical setting. BLI technology offered robust measurements of dynamic disease progression and allowed for objective evaluation of the response to individual cancer agents in the MDA-MB-435-HAL-Luc SRC and MFP tumor models.

In summary, BLI is a sensitive tool for longitudinal assessment of tumors and metastases progression in living mice. Through BLI technology, we report that the MDA-MB-435-HAL-Luc SRC model displayed a higher metastatic potential compared with the MFP model. BLI allowed quantitative measurement of the antitumor and antimetastatic benefits of PD-0332991, docetaxel, and Avastin. By using optimized BLI technique, the clinically relevant disease models can be developed for efficient evaluation of drug effects, thereby allowing scientists to gain deeper knowledge of the underlying biology during disease progression and to accelerate cancer drug discovery.

Disclosure of Potential Conflicts of Interest

The authors were employed by Pfizer, Inc. at the time of the study.

References

1. Sawyer TK. Cancer metastasis therapeutic targets and drug discovery: emerging small-molecule protein kinase inhibitors. Expert Opin Investig Drugs 2004;13:1–19.
2. Fidler IJ. The pathogenesis of cancer metastasis: the 'seed and soil' hypothesis revisited. Nat Rev Cancer 2003;3:453–8.
3. McCar thy N. To grow and spread. Nat Rev Drug Discov 2007;6:346–7.
4. Khanna C, Hunter K. Modeling metastasis *in vivo*. Carcinogenesis 2005;26:513–23.
5. Welch DR. Technical considerations for studying cancer metastasis *in vivo*. Clin Exp Metastasis 1997;15:272–306.
6. Bruns C, Harbison MT, Kuniyasu H, Eue I, Fidler IJ. *In vivo* selection and characterization of metastatic variants from human pancreatic adenocarcinoma by using orthotopic implantation in nude mice. Neoplasia 1999;1:50–62.
7. Hoffman RM. Orthotopic metastatic mouse models for anticancer drug discovery and evaluation: a bridge to the clinic. Invest New Drugs 1999;17:343–60.
8. Flatmark K, Mlandsmo GM, Martinsen M, Rasmussen H, Fodstad Ø. Twelve colorectal cancer cell lines exhibit highly variable growth and metastatic capacities in an orthotopic model in nude mice. Eur J Cancer 2004;40:1593–8.
9. Morimoto-Tomita M, Ohashi Y, Matsubara A, Tsuiji M, Irimura T. Mouse colon carcinoma cells established for high incidence of experimental hepatic metastasis exhibit accelerated and anchorage-independent growth. Clin Exp Metastasis 2005;22:513–21.
10. Man S, Munoz R, Kerbel R. On the development of models in mice of advanced visceral metastatic disease for anti-cancer drug testing. Cancer Metastasis Rev 2007;26:737–47.
11. Fidler IJ. Models for spontaneous metastasis. Cancer Res 2006;66:9787.
12. Ross DT, Scherf U, Eisen MB, et al. Systematic variation in gene expression patterns in human cancer cell lines. Nat Genet 2000;24:227–35.
13. Brinkley BR, Beall PT, Wible LJ, Mace ML, Turner

DS, Cailleau RM. Variations in cell form and cytoskeleton in human breast carcinoma cells *in vitro*. Cancer Res 1980;40:3118–29.

14. Cailleau R, Olivé M, Cruciger QV. Long-term human breast carcinoma cell lines of metastatic origin: preliminary characterization. In Vitro Cellular Devel Biol Plant 1978;14:911–5.

15. Sellappan S, Grijalva R, Zhou X, et al. Lineage infidelity of MDA-MB-435 cells: expression of melanocyte proteins in a breast cancer cell line. Cancer Res 2004;64:3479–85.

16. Price JE, Zhang RD. Studies of human breast cancer metastasis using nude mice. Cancer Metastasis Rev 1990;8:285–97.

17. Vantyghem SA, Wilson SM, Postenka CO, Al-Katib W, Tuck AB, Chambers AF. Dietary genistein reduces metastasis in a postsurgical orthotopic breast cancer model. Cancer Res 2005;65:3396–403.

18. Schmidt C, Settle S, Keene J, Westlin W, Nickols G, Griggs D. Characterization of spontaneous metastasis in an aggressive breast carcinoma model using flow cytometry. Clin Exp Metastasis 1999; 17:537–44.

19. Murray L, Abrams T, Long K, et al. SU11248 inhibits tumor growth and CSF-1R-dependent osteolysis in an experimental breast cancer bone metastasis model. Clin Exp Metastasis 2003;20:757–66.

20. Chang Y-F, Lin Y-Y, Wang H-E, Liu R-S, Pang F, Hwang J-J. Monitoring of tumor growth and metastasis potential in MDA-MB-435s/tk-luc human breast cancer xenografts. Nuclear Instruments and Methods in Physics Research Section A: Accelerators, Spectrometers, Detectors and Associated Equipment 2007;571:155–9.

21. Waalkes MP, Diwan BA. Cadmium-induced inhibition of the growth and metastasis of human lung carcinoma xenografts: role of apoptosis. Carcinogenesis 1999;20:65–70.

22. Bogden AE, Cobb WR, Lepage DJ, et al. Chemotherapy responsiveness of human tumors as first transplant generation xenografts in the normal mouse: six-day subrenal capsule assay. Cancer 1981;48:10–20.

23. Aamdal S, Fodstad O, Pihl A. The six-day subrenal capsule assay (SRCA) for testing the response of human tumours to anticancer agents. Validity and usefulness in cancer research and treatment. Ann Chir Gynaecol Suppl 1985;199:51–9.

24. Stratton JA, Kucera PR, Micha JP, et al. The subrenal capsule tumor implant assay as a predictor of clinical response to chemotherapy: 3 years of experience. Gynecol Oncol 1984;19:336–47.

25. Hahka-Kemppinen M, Muhonen T, Kangas L, Pyrhönen S. Chemosensitivity of human melanoma metastases in mouse subrenal capsule assay-can it predict tumour response to combined cytostatic plus interferon therapy in metastatic melanoma? Melanoma Res 1996;6:215–21.

26. Kaijzel EL, van der Pluijm G, Lowik CWGM. Whole-body optical imaging in animal models to assess cancer development and progression. Clin Cancer Res 2007;13:3490–7.

27. Deroose CM, De A, Loening AM, Chow PL, Ray P, Chatziioannou AF, Gambhir SS. Multimodality imaging of tumor xenografts and metastases in mice with combined small-animal PET, small-animal CT, and bioluminescence imaging. J Nucl Med 2007;48:295–303.

28. Ntziachristos V. Fluorescence molecular imaging. Annu Rev Biomed Eng 2006;8:1–33.

29. Hoffman RM. The multiple uses of fluorescent proteins to visualize cancer *in vivo*. Nat Rev Cancer 2005; 5:796–806.

30. Montet X, Ntziachristos V, Grimm J, Weissleder R. Tomographic fluorescence mapping of tumor targets. Cancer Res 2005;65:6330–6.

31. Troy T, Jekic-McMullen D, Sambucetti L, Rice B. Quantitative comparison of the sensitivity of detection of fluorescent and bioluminescent reporters in animal models. Mol Imaging 2004;3:9–23.

32. Henriquez NV, van Overveld PGM, Que I, et al. Advances in optical imaging and novel model systems for cancer metastasis research. Clin Exp Metastasis 2007;24:699–705.

33. Licha K, Olbrich C. Optical imaging in drug discovery and diagnostic applications. Adv Drug Deliv Rev 2005;57:1087–108.

34. Fry DW, Harvey PJ, Keller PR, et al. Specific inhibition of cyclin-dependent kinase 4/6 by PD 0332991 and associated antitumor activity in human tumor xenografts. Mol Cancer Ther 2004;3: 1427–38.

35. Zou HY, Li Q, Lee JH, et al. An orally available small-molecule inhibitor of c-Met, PF-2341066, exhibits cytoreductive antitumor efficacy through antiproliferative and antiangiogenic mechanisms. Cancer Res 2007;67:4408–17.

36. Contag PR. Unraveling the complexicity of oncogenesis through *in vivo* optical imaging. In: LaRochelle WJ, Shimkets RA, editors. Cancer Drug Discovery and Development: the Oncogenomics Handbook. Humana Press; 2005. Chapter 17. p. 263–74.

37. Edinger M, Cao Ya, Hornig YS, et al. Advancing animal models of neoplasia through *in vivo* bioluminescence imaging. Eur J Cancer 2002;38: 2128–36.

38. Sarraf-Yazdi S, Mi J, Dewhirst MW, Clary BM. Use of *in vivo* bioluminescence imaging to predict hepatic tumor burden in mice. J Surg Res 2004; 120:249–55.

39. Paroo Z, Bollinger RA, Braasch DA, et al. Validating bioluminescence imaging as a high-throughput, quantitative modality for assessing tumor burden. Mol Imaging 2004;3:117–24.

40. Lee KH, Byun SS, Paik JY, et al. Cell uptake and tissue distribution of radioiodine labelled D-luciferin: implications for luciferase based gene imaging. Nucl Med Commun 2003;24:1003–9.

41. Anda P, Viktor N, Martina M, et al. MRI monitoring of Avastin™ antiangiogenesis therapy using B22956/1, a new blood pool contrast agent, in an experimental model of human cancer. J Magn Reson Imaging 2004;20:865–73.

42. Morse DL, Gray H, Payne CM, Gillies RJ. Docetaxel induces cell death through mitotic catastrophe in human breast cancer cells. Mol Cancer Ther 2005;4: 1495–504.

43. Bissery MC. Preclinical pharmacology of docetaxel. Eur J Cancer 1995;31:S1–6.